Journal of Solid State Chemistry **167,** 137–144 (2002)
doi:10.1006/jssc.2002.9635

Insights on the Structural Chemistry of Hydrocalumite and Hydrotalcite-like Materials: Investigation of the Series $Ca_2M^{3+}(OH)_6Cl \cdot 2H_2O$ (M^{3+}: Al^{3+}, Ga^{3+}, Fe^{3+}, and Sc^{3+}) by X-Ray Powder Diffraction

Isabelle Rousselot,* Christine Taviot-Guého,*,[1] Fabrice Leroux,* Philippe Léone,† Pierre Palvadeau,† and Jean-Pierre Besse*

*Laboratoire des Matériaux Inorganiques, UMRCNRS 6002, Université Blaise Pascal, 63177 Aubière Cédex, France; and †Institut des Matériaux Jean Rouxel, UMRCNRS 6502, BP 32229, 44322 Nantes Cédex 3, France

Hydrotalcite and hydrocalumite are two close minerals belonging to the layered double hydroxide family. Both structures are based on positive brucite-like layers alternating with layers containing anions and water molecules. Most of synthetic (LDHs) are hydrotalcite-like materials. On the other hand, the hydrocalumite structure type is rare for those less broad in composition, typically Ca^{2+} and Al^{3+} in the hydroxide layers. In order to get further insight into the conditions of stabilization of this structure type, we have undertaken the synthesis and the structural characterization by powder X-ray diffraction of the series $Ca_2M^{3+}(OH)_6Cl \cdot 2H_2O$($M^{3+}$: Al^{3+}, Ga^{3+}, Fe^{3+} and Sc^{3+}). The incorporation of Sc^{3+} ions is quite original. All phases crystallize in the rhombohedral space group *R*-3 resulting in a three-layers polytype. The main consequence of the replacement of Al^{3+} cations by large M^{3+} cations is a compression of the octahedral layers like it proceeds in hydrotalcite-like materials. The existence of Sc-containing phase allows us to say that it is the size of Ca^{2+} ions and the pronounced anisotropy of coordination spheres around Ca^{2+} and M^{3+} which are responsible for the ordered distribution of cations in hydrocalumite-like materials. © 2002 Elsevier Science (USA)

Key Words: **hydrocalumite; cement; structure; hydrotalcite; layered double hydroxides.**

INTRODUCTION

Already composed of a great number of members, the literature on anionic clays, also known as layered double hydroxides (LDHs), is being continuously enlarged with new data on natural and synthetic varieties (1–4). Their layered crystal structure is built by periodical stacking of positively charged $(M^{2+},M^{3+})(OH)_6$ octahedral layers related to brucite $Mg(OH)_2$ and negatively charged interlayers consisting of anions and water molecules. This unique structural character can be expressed by the general formula $[M_x^{2+}M^{3+}(OH)_{2x+2}]^+[A_{1/n}^{n-} \cdot mH_2O]^-$, abbreviated hereafter as $[M^{2+}$–M^{3+}–$A^{n-}]$, where M^{2+}/M^{3+} are divalent and trivalent cations, A an n-valent anion and x the M^{2+}/M^{3+} molar ratio. Though LDHs are rare in nature compared to cationic clays, they are relatively simple and inexpensive to prepare. Furthermore, their large range of composition and the high number of preparation variables make it possible to produce tailor-made materials resulting in substantial academic and industrial interest, mainly in the field of heterogeneous catalysis and environment (5–8). On the other hand, as is the case with many other layered solids, the layered structure of anionic clays is prone to form stacking faults producing crystals of different polytypes. The combination of these many variable properties probably accounts for the abundance of varieties within this group of minerals. Most of the synthetic LDHs resemble the naturally occurring hydrotalcite, $Mg_6Al_2(OH)_{16}CO_3 \cdot 4H_2O$, and have been studied extensively (9–12). The main features of hydrotalcite-like materials are a large chemical variation and a random distribution of cations within the octahedral layers. On the other hand, hydrocalumite-like materials are rare in the LDH family for those less broad in composition (13–22). The structure is based on corrugated brucite-like main layers with an ordered arrangement of Ca^{2+} and M^{3+} ions, seven-and six-coordinated, respectively, in a fixed ratio of 2:1; the seventh apex of the Ca-polyhedron is a water molecule from the interlayer. The general formula of this group is $[Ca_2M^{3+}(OH)_6]^+[A_{1/n}^{n-} \cdot mH_2O]^-$. The composition of the hydroxide layer of this structure type is limited; the divalent and trivalent cations are typically Ca^{2+} and Al^{3+}. These lamellar calcium aluminum hydroxides salts have been studied in detail for they occur in the hydration process of cement compounds (23, 24). The

[1] To whom correspondence should be addressed. E-mail: gueho@chimtp.univ-bpclermont.fr.

0022-4596/02 $35.00

replacement of Al^{3+} by Fe^{3+}, Cr^{3+}, Ga^{3+}, and Ca^{2+} by Cd^{2+} have been reported but only few data are available on these phases (25–27). In spite of this lack of information, it is widely assumed that the difference in size between Ca^{2+} and M^{3+} ions is responsible for their ordered arrangement in a fixed $M^{2+}:M^{3+}$ ratio of 2:1. Conversely, close cation radii in hydrotalcite-like materials enable a joint replacement and a large chemical variation.

The present paper aims at a detailed description of a series of hydrocalumite-like materials, $Ca_2M^{3+}(OH)_6Cl\cdot 2H_2O$ with $M^{3+}Al^{3+}$, Sc^{3+}, Fe^{3+}, and Ga^{3+} in order to get further insight into the conditions of stabilization of this structure type. The incorporation of Sc^{3+} ions is quite original. All these phases were prepared within 2 days by the coprecipitation method at controlled pH in water ethanol medium. To the best of our knowledge, there is no report in the literature of such preparative procedure of hydrocalumite-like materials usually obtained by hydrothermal synthesis over a period of 1 month at least. The good crystallinity of the final products allowed us to perform a structural study by Rietveld refinement of X-ray diffraction diagrams.

EXPERIMENTAL SECTION

Synthesis

The compounds were prepared by the coprecipitation method (28) at controlled pH, using deionized and decarbonated water and under nitrogen atmosphere in order to avoid contamination by carbonate anions. The synthesis of [Ca–Al–Cl] and [Ca–Ga–Cl] compounds was performed at 65°C whereas a better crystallinity was obtained at room temperature for [Ca–Fe–Cl] and [Ca–Sc–Cl]. Typically, 10 mL of a mixed solution of 0.66 M $CaCl_2$ and 0.33 M $M^{3+}Cl_3$ (or $M^3(NO_3)_3$) were added dropwise to a reactor, the pH being kept constant at 11.5 ± 0.1 by the simultaneous addition of 2.0 M NaOH solution. In the case of [Ca–Fe–Cl], the reacting flask was previously filled with 250 mL of water while a mixture of the same volume consisting of water and ethanol in a 2:3 volumetric ratio was used for the other compositions. The synthesis of Ga-and Sc-containing samples being carried out with the nitrate salts $Ga(NO_3)_3$ and $Sc(NO_3)_3$, before starting the addition, a few drops of 1 M HCl were added to the reaction mixture up to a pH value of 4 as a source of chloride anions.

After complete addition of the metallic salts, the precipitate was aged in the mother solution for 24 h at the same temperature as the synthesis. The crystallites were then isolated by two centrifugation cycles, dried at room temperature under dynamic vacuum and finally stored in a CO_2-free atmosphere.

The chemical analysis was performed at the Vernaison Analysis Center of CNRS (Table 1).

Structural Study

Powder X-Ray Diffraction

The powder X-ray diffraction patterns were collected at room temperature in the Debye–Scherrer geometry for 12 h using an INEL CPS120 detector. Monochromatized $CuK\alpha_1$ radiation was used. The powders were put in 0.5 mm diameter capillary. This capillary preparation reduces preferred orientation but introduces sample absorption effects, hence intensities were corrected for absorption in the case of gallium- and iron-containing samples. The program FULLPROF (29) was used for the Rietveld procedure. The intensities of the reflections were calculated using the analytical Thompson–Cox–Hasting pseudo-Voigt peak-shape function (30); the background was defined by linear interpolation between points in the patterns. The structural refinements were carried out in the angular range 9.5–90.0 (2θ), starting from the atomic positions of the mineral $Ca_2Al(OH)_6\cdot\frac{1}{2}SO_4^{2-}\cdot 2H_2O$ as a structural model (13) and crystallizing in R-3 space group. The final refinements of the atomic positions, along with the scale factor and the profile parameters led to good R-factor values gathered in Table 2. The isotropic atomic displacement factors were not refined; the values are those reported in the literature determined on a single crystal of $Ca_2Al(OH)_6Cl\cdot 2H_2O$ crystallizing in the space group R-3c (20).

TABLE 1
Chemical Composition

Sample	Ca/M^{3+} molar ratio	Cl^-/M^{3+} molar ratio	C content wt%	H content wt%	Formulas[a]
[Ca–Al–Cl]	2.01	1.00	1.24	3.53	$Ca_2Al(OH)_6Cl\cdot 2H_2O$ 0.29 H_2O 0.31CO_2
[Ca–Ga–Cl]	2.07	0.95	1.03	2.99	$Ca_2Ga(OH)_6Cl\cdot 2H_2O$ 0.05 H_2O 0.29CO_2
[Ca–Fe–Cl]	2.00	1.01	0.94	3.07	$Ca_2Fe(OH)_6Cl\cdot 2H_2O$ 0.25CO_2

[a] Physisorbed species in italic.

TABLE 2
Rietveld Refinement Results

	$Ca_2Al(OH)_6Cl\cdot 2H_2O$	$Ca_2Ga(OH)_6Cl\cdot 2H_2O$	$Ca_2Fe(OH)_6Cl\cdot 2H_2O$
Formula weight	280.59	323.33	697.8(2)
Space group	*R*-3	*R*-3	*R*-3
Lattice parameters			
a (Å)	5.7487(5)	5.8262(5)	5.873(1)
c (Å)	23.492(1)	23.417(1)	309.45
Volume (Å^3)	672.32(9)	688.4(1)	23.362(2)
Z	3	3	3
Temperature (K)	293	293	293
λCu$K\alpha_1$ (Å)	1.540598	1.540598	1.540598
R_{wp}(%)	2.79/11.3(BC)[a]	3.22/11.5(BC)[a]	1.26/11.0(BC)[a]
χ^2	7.68	7.94	5.50

[a] BC, background corrected.

X-Ray Absorption Spectroscopy

Ca and Sc *k-edges* XAS study was performed at LURE (Orsay, France) using X-ray synchrotron radiation emitted by the DCI storage ring (1.85 GeV positrons, average intensity of 250 mA) at the D44 beam line. Powders were finely dispersed in ethanol and then deposited on membrane. Data were collected at room temperature in transmission mode at Ca and Sc *k-edges* (4038.1 and 4492.8 eV, respectively). A double-crystal Si (111) monochromator scanned the energy in 2 eV-steps from 3900 to 5300 eV, with a two-mirror device for harmonic rejection (detuning of 30% in intensity). Three spectra were recorded for each sample and an accumulation time of 2 s was used per point. Extraction and analysis of EXAFS data were performed following standard procedures as reported elsewhere (31). The $\chi(k)$ signal was fitted by using the classical plane-wave single scattering approximation: $\chi(k) = S_0^2 \sum A_i(k)\sin[2kr_i + \phi_i(k)]$, with $A_i(k)$ amplitude being equal to $(N_i/kr_i^2)F(k)\exp(-2k^2\sigma_i^2)$, where r_i is the interatomic distance, ϕ_i the total phase shift of the ith shell, N_i the effective coordination number, σ_i the Debye–Waller factor and $F_i(k)$ the backscattering amplitude. The residual ρ factor is defined as $\rho = [\sum(k^3\chi_{exp}(k) - k^3\chi_{theo}(k))^2 / \sum(k^3\chi_{exp}(k))^2]^{1/2}$. The commonly accepted fitting accuracy is of about 0.02 Å for the distance and $\approx$20% for the number of neighbors.

RESULTS AND DISCUSSION

The chemical composition of the compounds investigated are reported in Table 1. As expected, the Ca^{2+}/M^{3+} ratio is equal to 2. It is worth noting that the amount of chloride anions exactly balances the positive charge of the main layer thus excluding the presence of carbonates species in the interlamellar space. Hence, detected carbon is likely to be due to physisorbed CO_2 on the outer surface of the crystallites as often reported for LDHs owing to their basic character (32). The analyses also show the presence of small amounts of physisorbed water.

Powder X-ray diffraction (PXRD) patterns presented in Fig. 1 are typical of layered compounds with maximum intensity for the (00l) reflections at low 2θ values. All compounds present similar X-ray diagrams suggesting isostructural structures. Furthermore, the symmetry and relative sharpness of the reflections indicate the absence of stacking faults except for Sc-containing sample exhibiting a poorer crystallinity (Fig. 1d).

Structural parameters are given in Table 3, selected bond distances and angles are listed in Table 4. The observed, calculated and difference profiles are displayed in Fig. 1.

All PXRD patterns can be indexed in a hexagonal lattice with an *R*-3 rhombohedral symmetry. The present refinements being the first made on this space group, with chloride anions in the interlamellar space, a brief review of the literature on the crystal chemistry of hydrocalumite is necessary.

Several rhombohedral space groups *R*-3 (13, 17)/*R*-3*c* (20)/*P*-3*c*1 (19), a monoclinic one *C*2/*c* (14, 15) and the two triclinic space groups *P*1, *P*-1 (17, 21) have been observed for synthetic monoanionic tetracalcium aluminates.

In the rhombohedral space groups *R*-3 and *R*-3c, the water molecules linked to Ca atoms are on the straight line passing through the Ca atoms and perpendicular to the (001) plane (Fig. 2). Besides, the neighboring brucite-like layers may be stacked in two different ways building two kinds of interlayers: either OH groups form prisms resulting in a three-layer polytype (3*R*) and the *R*-3 unit cell or they form octahedra resulting in a six-layer polytype (6*R*) and the *R*-3c unit cell. As already noticed by Sacerdoti and Passaglia (16) and more recently by Rapin (33), the change of space group from *R*-3 to *R*-3c depends on the size of the anions. Indeed, chloride compound crystallizes in the space group *R*-3c, larger anions like iodine and sulfate compounds crystallize in *R*-3 while intermediate anions like bromide exhibits the two unit cells. The same

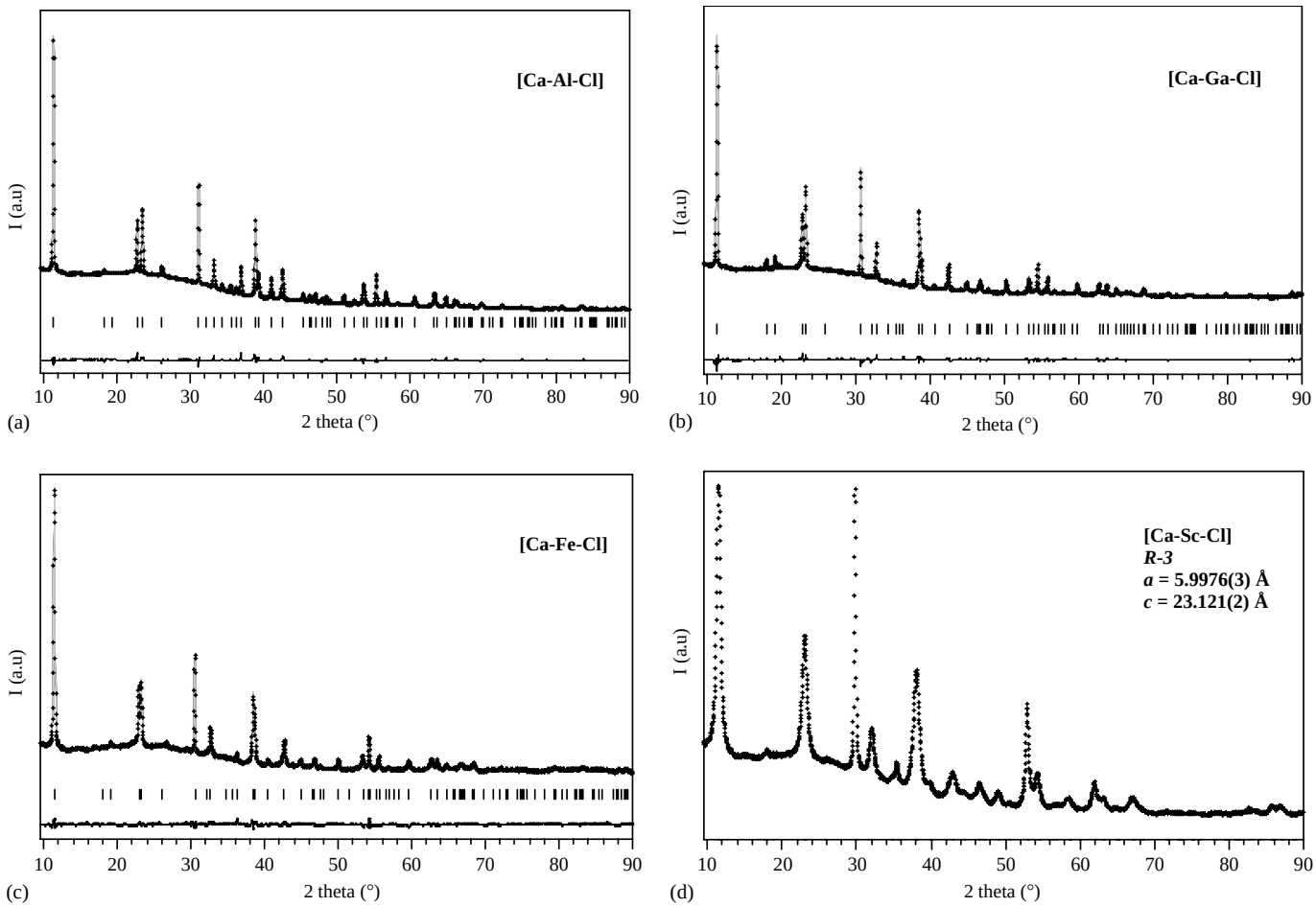

FIG. 1. Experimental X-ray diffraction pattern (cross), calculated (line), Bragg reflections (ticks) and difference profiles for (a) [Ca–Al–Cl], (b) [Ca–Al–Cl] and (c) [Ca–Fe–Cl]. (d) [Ca–Sc–Cl] experimental data and least-squares refinement results.

authors have also shown that these rhombohedral phases are actually high-temperature phases characterized by a disruption of the hydrogen bonds between interlayer species. Their restoration at low temperature results in a monoclinic or triclinic distortion with a displacement of water molecules linked to Ca atoms towards interlayer anions. This structural phase transition occurs near room temperature and has only been observed with halogenous anions, so far. In this way, the monoclinic ($C2/c$) chloride compound reversibly transforms at 28°C in the rhombohedral space group R-3c. Finally, the symmetry of the crystal may also depend on the synthesis conditions. For instance, the tetracalcium monocarboaluminate (17, 21) obtained by hydrothermal synthesis crystallizes in two space groups depending on the temperature: when the synthesis is carried out at 100°C, the interlayer space is disordered and the structure is centrosymmetric P-1, while at 120°C the structure is completely ordered and noncentrosymmetric P1. Another particularity of these carbonate phases, also exhibited by nitrate phases (19), is the partial replacement of the water molecules linked to Ca atoms by carbonate or nitrate anions.

Thus, according to the literature, the present Cl compounds should crystallize either in the $C2/c$ or the R-3c space group. It is clear that Bragg peaks cannot be indexed in the monoclinic cell. On the other hand, the difference between R-3 and R-3c powder diffraction patterns is less evident for practically only one additional peak is expected in R-3c (20) of rather weak intensity and corresponding to diffraction from the (113) plane (Fig. 3). This reflection is not visible here but its occurrence may strongly depend on the degree of crystallinity of the powder. However, attempts of refinement in the space group R-3c led to high values of R-factors with convergence problems even in the presence of strong constraints on the interatomic distances. Though contrasting with the above-stated rules, the R-3 structural model is supported by satisfactory R-factor values and may be related to the synthesis conditions which are original for this family of compounds.

TABLE 3
Positional Parameters

Atom	Site	x	y	z	B_{iso}(Å^2)
			$Ca_2Al(OH)_6Cl \cdot 2H_2O$		
Ca	6(*c*)	$\frac{2}{3}$	$\frac{1}{3}$	0.02531(9)	1.1
Al	3(*a*)	0	0	0	1.3
OH	18(*f*)	0.2525(7)	−0.0580(6)	0.0430(1)	1.3
Cl	3(*b*)	0	0	$\frac{1}{2}$	5.3
H_2O	6(*c*)	$\frac{2}{3}$	$\frac{1}{3}$	0.1334(3)	4.3
			$Ca_2Ga(OH)_6Cl \cdot 2H_2O$		
Ca	6(*c*)	$\frac{2}{3}$	$\frac{1}{3}$	0.0250(1)	1.1
Ga	3(*a*)	0	0	0	1.3
OH	18(*f*)	0.2658(9)	−0.0495(9)	0.0428(1)	1.3
Cl	3(*b*)	0	0	$\frac{1}{2}$	5.3
H_2O	6(*c*)	$\frac{2}{3}$	$\frac{1}{3}$	0.1344(3)	4.3
			$Ca_2Fe(OH)_6Cl \cdot 2H_2O$		
Ca	6(*c*)	$\frac{2}{3}$	$\frac{1}{3}$	0.0250(1)	1.1
Ga	3(*a*)	0	0	0	1.3
OH	18(*f*)	0.282(1)	−0.064(1)	0.0383(1)	1.3
Cl	3(*b*)	0	0	$\frac{1}{2}$	5.3
H_2O	6(*c*)	$\frac{2}{3}$	$\frac{1}{3}$	0.1313(4)	4.3

Before considering the consequences of the replacement of Al^{3+} cations by larger M^{3+} cations, it is worthwhile to compare the structure of $Ca_2Al(OH)_6 \cdot Cl \cdot 2H_2O$ with the equivalent sulfate (13) and iodide (18) compounds. All crystallize in the same space group *R*-3 which means a rhombohedral stacking of three octahedral layers and water molecules on the ternary axis passing through Ca atoms. Like I^- monovalent anions, Cl^- anions fully occupy the position 3(b) leading to completely ordered structures while sulfate groups share this position with water molecules. In the layers, the Ca–OH distances are similar in the three phases. As commonly observed in LDHs, $Al^{3+}(OH)_6$ octahedra are compressed in the *c* direction (10). Though the distortion is the same in the three phases, the Al^{3+}–OH bond length in [Ca–Al–Cl], 1.929(3) Å, is much higher than that reported for [Ca–Al–SO_4] and [Ca–Al–I] with 1.909 Å in both cases, and results in an increase in the *a* parameter. The Ca–H_2O distance is also longer 2.540(7) Å against 2.441(9) Å in [Ca–Al–I] and 2.497(3) Å in [Ca–Al–SO_4] and may be explained by the high electronegativity of chloride anions tearing water molecules from Ca atoms.

The comparison of the present [Ca–Al–Cl] compound with compounds of the same composition but crystallizing in *R*-3*c* (20) and *C*2/*c* (14, 33) space groups shows somewhat intermediate bond lengths in the *R*-3 space group, with distances in the main layer close to those observed in the *C*2/*c* space group whereas the Cl–H_2O/OH distances correspond to those of the *R*-3*c* space group.

The replacement of Al^{3+} cations by larger M^{3+} cations results in a linear variation of the unit-cell parameters presented in Fig. 4: *a* increases and *c* decreases as the M^{3+}–OH bond length increases. In the octahedral layer, the accommodation of longer M^{3+}–OH distances proceeds like in hydrotalcite-like compounds i.e., by a flattening of $M^{3+}(OH)_6$ octahedra along the *c*-axis in order to minimize the repulsion between cations (10). This distortion evidenced by the HO–M^{3+}–OH bond angle values given in Table 4 goes along with a contraction of the surrounding

TABLE 4
Bond Lengths (Å) and Angles (°)

	$Ca_2Al(OH)_6Cl \cdot 2H_2O$	$Ca_2Ga(OH)_6Cl \cdot 2H_2O$	$Ca_2Fe(OH)_6Cl \cdot 2H_2O$
M^{3+}–OH (× 6)	1.929(3)	1.983(5)	2.074(7)
Ca–OH (× 3)	2.355(4)	2.323(5)	2.277(6)
(× 3)	2.455(4)	2.463(5)	2.321(7)
Ca–H_2O	2.540(7)	2.561(8)	2.510(9)
Cl–OH (× 6)	3.449(3)	3.457(4)	3.474(5)
Cl–H_2O (× 6)	3.409(2)	3.447(2)	3.489(2)
M^{3+}– Cl	3.915	3.903	3.892
OH–H_2O	3.144(5)	3.133(7)	3.162(8)
Layer thickness	2.02	2.00	1.78
Interlayer thickness	5.81	5.80	5.99
OH–M^{3+}–OH	84.9(2)	83.3(3)	77.2(4)
	95.1(3)	96.7(4)	102.8(6)
	180.0(3)	180.0(5)	180.0(7)
OH –Ca– OH	65.5(2)	66.8(2)	68.5(3)
	81.9(2)	83.8(3)	78.2(4)
	116.9(3)	116.8(4)	117.9(5)
	146.5(3)	148.1(4)	148.1(5)
OH–Ca–H_2O	79.8(2)	79.6(3)	81.6(4)
	130.8(3)	130.2(4)	129.6(5)

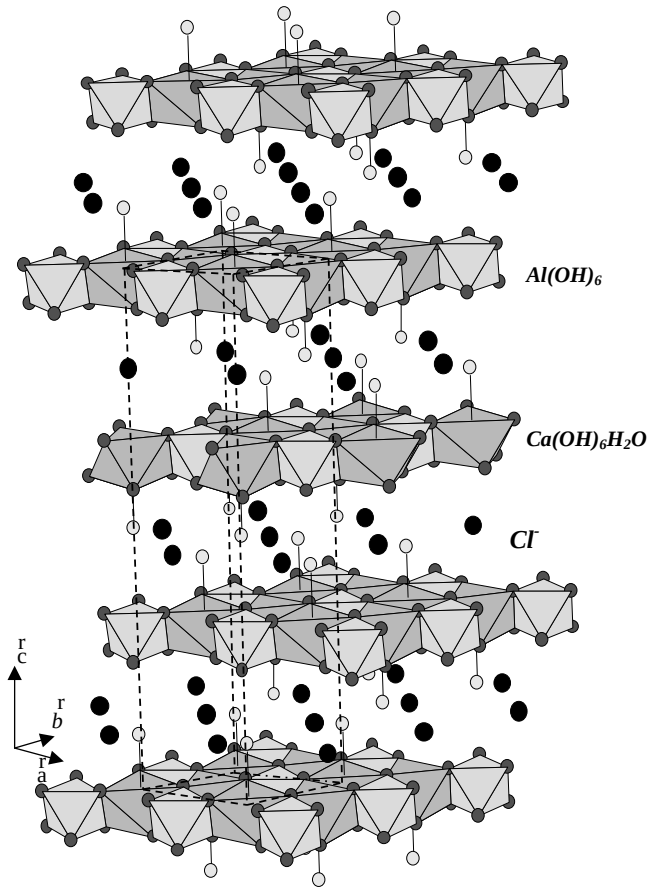

FIG. 2. Crystal structure of $Ca_2Al(OH)_6 \cdot Cl, 2H_2O$ in *R*-3 space group.

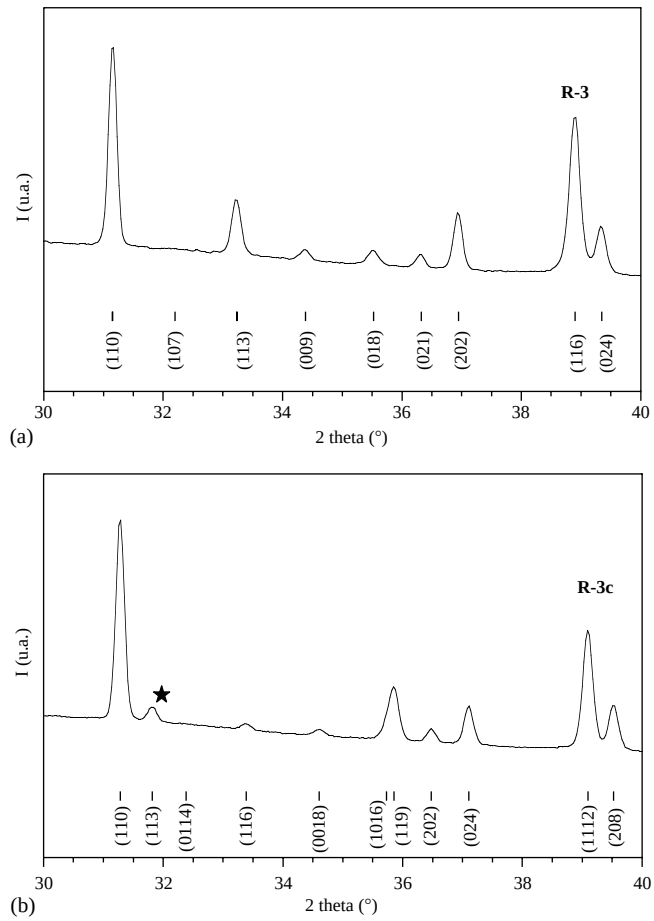

FIG. 3. Comparison of the PXRD patterns of $Ca_2Al(OH)_6 \cdot Cl \cdot 2H_2O$ in a) *R*-3 (present data) and (b) *R*-3*c* space groups (calculated from ref. (32).

$Ca(OH)_6H_2O$ polyhedra: Ca atoms near the center of their $(OH)_6$ octahedra and both the Ca–OH and Ca–H_2O distances decrease. The overall effect on these octahedral layers is thus a compression in the *c* direction and an elongation in the (*a*, *b*) plane.

In the interlamellar space, the Cl–OH/H_2O and OH–H_2O distances are consistent with the existence of hydrogen bond network connecting the layers. The OH groups and the water molecules of neighboring layers form trigonal antiprisms around the chloride anions leading to a coordination of 12. Cl^- anions are located at mid-distance between two successive layers on the ternary axis passing through the M^{3+} ions. The deformation of the octahedral layers tears OH groups and even more the water molecules from the Cl^- anions. On the other hand, the M^{3+}–Cl bond length scarcely changes. Accordingly, the decrease of the *c* parameter is mainly attributed to the decrease of the octahedral layer thickness.

As already said, the anisotropic line broadening in the diffraction pattern of [Ca–Sc–Cl] ascribed either to stacking faults, particle size or strain effects makes it impossible to solve the structure of this compound. Yet, the resemblance between X-ray diagrams indicates a similar structure; the unit-cell parameters of [Ca–Sc–Cl] were obtained from a least-squares refinement of *d*-spacings: $a = 5.9976(3)$ and $c = 23.121(2)$ Å.

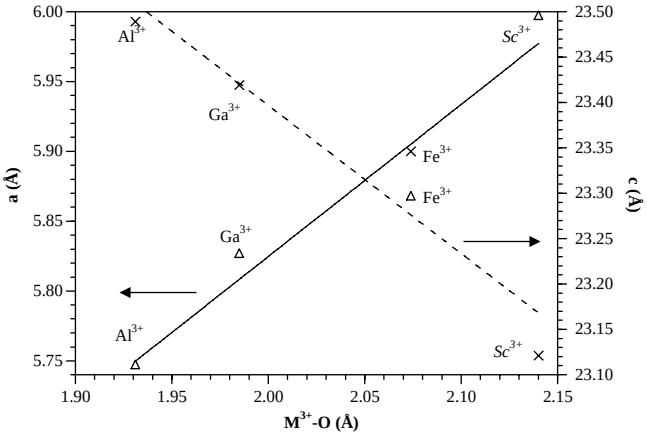

FIG. 4. Lattice parameters *a* and *c* as a function of M^{3+}–O bond length.

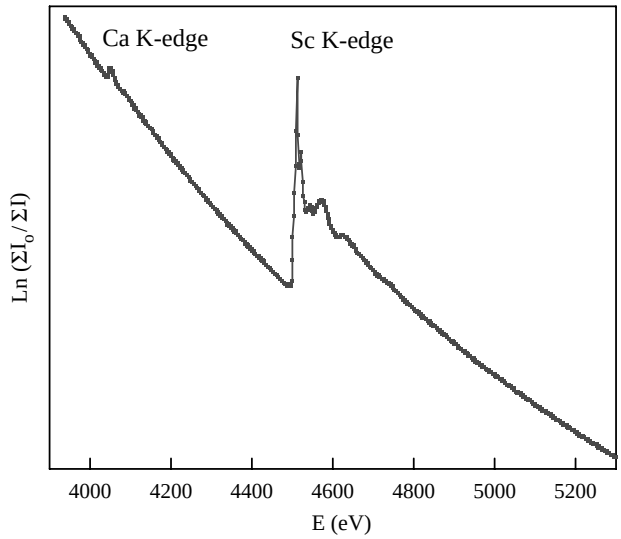

FIG. 5. EXAFS spectra for [Ca–Sc–Cl] sample.

To get a better picture from the [Ca–Sc–Cl] structure, EXAFS study was performed to access the local environment information. EXAFS spectrum is provided in Fig. 5. Sc_2O_3, which crystallizes in the *Ia*-3 space group with a parameter *a* of 9.849 Å, was used as reference compound (34). The refinements agree well with the crystallographic data. Concerning Sc *k*-edge, the moduli of the Fourier transforms are displayed in Fig. 6a. The first peak is characteristic of the oxygen atoms shell. In octahedral coordination in the reference sample, this contribution is similar in [Ca–Sc–Cl]; the Sc–O distance was refined at 2.14 Å ($N = 6.1$), associated with a Debye–Waller factor of $\sigma^2 = 0.0055\,\text{Å}^2$ that may indicate a rigid oxygen cage around Sc atoms. This distance well agrees with the linear variation of the M^{3+}–O distance as a function of the lattice parameters, established above (Fig. 4). The metal-to-metal correlation distance is refined at 2.98 Å ($N = 4.5$) ($\sigma^2 = 0.01\,\text{Å}^2$) but it was not possible to determine the nature of the backscattering atoms, either Sc or Ca atoms (noted as *M*e). The quality of the fit is presented in the inset of Fig. 6a. This *M*e–*M*e distance leads to a value of 5.96 Å for the *a* parameter, consistent with the X-ray diffraction results. Inherent to the material, only qualitative results were gathered at Ca *k*-edge partly due to the small energy range available after the edge, as exemplified in Fig. 5. We were not able to refine clearly Ca *k*-edge EXAFS signal. Modulus of the Fourier transform is displayed in Fig. 6b.

To the best of our knowledge, the existence of [Ca–Sc–Cl] compound has never been reported so far. This phase brings more insight into the crystal chemistry of

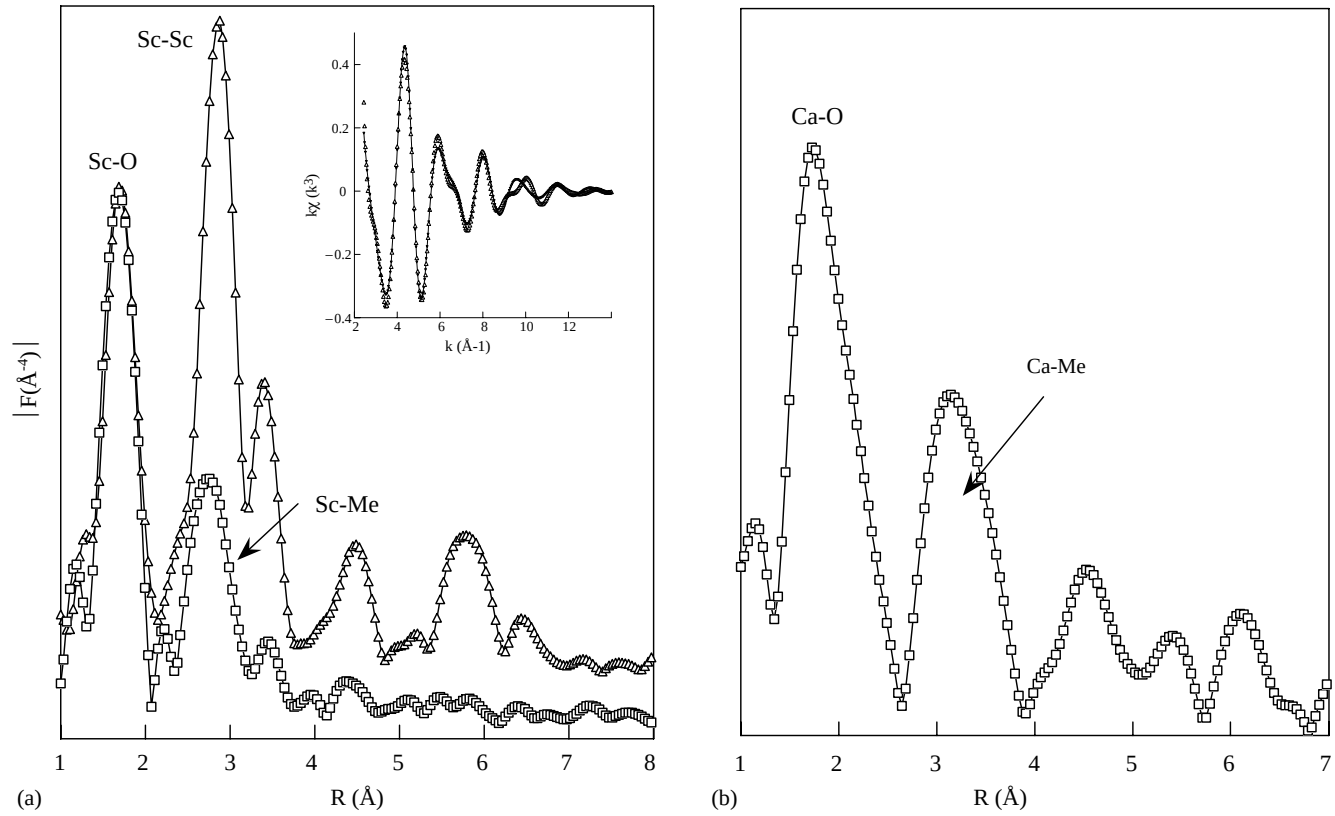

FIG. 6. Moduli of the Fourier transform: (a) at Sc *k*-edge, triangle dots for Sc_2O_3 and square dots for hydrocalumite phase (the refinement of [Ca–Sc–Cl] is provided in inset); (b) Ca *k*-edge. The distances are not corrected from phase shifts.

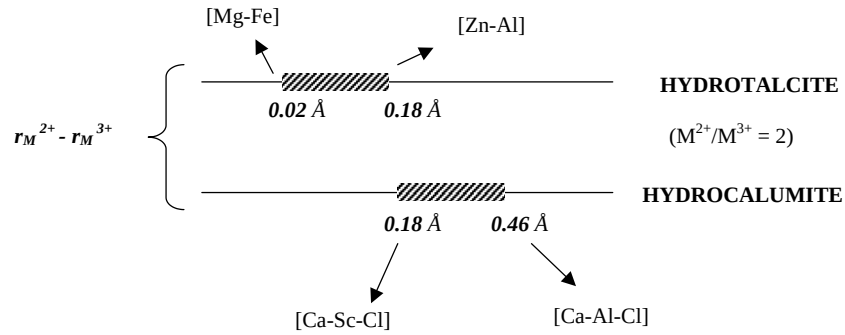

FIG. 7. Ionic radii (Pauling) differences observed in octahedral layers of hydrotalcite and hydrocalumite-like compounds for $M^{2+}/M^{3+} = 2$.

hydrotalcite- and hydrocalumite-like compounds. Until now, it was generally admitted that because of the large difference in size between the Ca^{2+} and Al^{3+} ions, the M^{2+}/M^{3+} ratio is fixed at 2 and their arrangement is ordered. Conversely, close cation radii would be responsible for the disorder in hydrotalcite-like materials. Figure 7 exhibits the range of stability, in terms of ionic radii ($rM^{2+} - rM^{3+}$), for both structure types with an M^{2+}/M^{3+} ratio equal to 2. In the case of hydrotalcite-like compounds, [Mg–Fe] and [Zn–Al] systems represent the lower and upper limits with a difference in size between M^{2+} and M^{3+} ions of 0.02 and 0.18 Å, respectively. Though limited in composition, the hydrocalumite structure type can accommodate a larger ionic radii difference in the octahedral layers, ranging from 0.46 Å for [Ca–Al] to 0.18 Å for [Ca–Sc]. The coincidence of this limit value at 0.18 Å for both series is quite remarkable. In our opinion, more than the difference in size between Ca^{2+} and M^{3+} ions, it is the size of Ca^{2+} and the pronounced anisotropy of coordination spheres around Ca^{2+} and M^{3+} which are responsible for the structural order in hydrocalumite-like compounds.

REFERENCES

1. H. F. W. Taylor, *Mineral. Mag.* **304,** 377–389 (1973).
2. W. Hofsmeister and H. Von Platen, *Cryst. Rev.* **3,** 3–29 (1991).
3. F. Trifiro and A. Vaccari, *in* "Comprehensive Supramolecular Chemistry" (J. L. Atwood, J. E. D. Davies, D. D. MacNicol, and F. Vogtle, Eds.), Vol. 7, p. 251. Pergamon, Oxford, 1996.
4. A. de Roy, *Mol. Cryst. Liq. Cryst.* **311,** 173–193 (1998).
5. V. Rives and M. A. Ulibarri, *Coord. Chem. Rev.* **181,** 61–120 (1999).
6. A. Vaccari, *Appl. Clay Sci.* **14,** 161–198 (1999).
7. M. A. Ulibarri, I. Pavlovic, M. C. Hermosin, and J. Cornejo, *Appl. Clay Sci.* **10,** 131–145 (1995).
8. J. Inacio, C. Taviot-Guého, C. Forano, and J. P. Besse, *Appl. Clay Sci.* **18,** 255–264 (2001).
9. A. S. Bookin and V. A. Drits, *Clays Clay Miner.* **5,** 551–564 (1993).
10. M. Belloto, B. Rebours, O. Clause, J. Lynch, D. Bazin, and E. Elkaïm, *J. Phys. Chem.* **20,** 8527–8534 (1996).
11. M. Vucelic, W. Jones, and G. D. Moggridge, *Clays Clay Miner.* **6,** 803–813 (1997).
12. H. Roussel, V. Briois, E. Elkaïm, A. de Roy, and J. P. Besse, *J. Phys. Chem. B* **25,** 5915–5923 (2000).
13. R. Allmann, *N. Jb. Miner. Mh.* 136–144 (1977).
14. A. Terzis and S. Philippakis, *Z. Kristallogr.* **181,** 29–34 (1987).
15. E. Passaglia and M. Sacerdoti, *N. Jb. Miner. Mh.* 454–461 (1988).
16. M. Sacerdoti and E. Passaglia, *N. Jb. Miner. Mh.* 462–475 (1988).
17. M. François, G. Renaudin, and O. Evrard, *Acta Crystallogr. C* **54,** 1214–1217 (1998).
18. J. P. Rapin, A. Walcarius, G. Lefèvre, and M. François, *Acta Crystallogr. C* **55,** 1957–1959 (1999).
19. G. Renaudin and M. François, *Acta Crystallogr. C* **55,** 835–838 (1999).
20. G. Renaudin, F. Kubel, J. P. Rivera, and M. François, *Cem. Concr. Res.* **29,** 1937–1942 (1999).
21. G. Renaudin, M. François, and O. Evrard, *Cem. Concr. Res.* **29,** 63–69 (1999).
22. G. Renaudin, J. P. Rapin, B. Humbert, and M. François, *Cem. Concr. Res.* **30,** 307–314 (2000).
23. V. Fernon, A. Vichot, P. Colombet, H. van Damme, and F. Bégin, *Mater. Sci. Forums* **152–153,** 335–338 (1994).
24. H. Kuzel and H. Baier, *Eur. J. Mineral.* **8,** 129–141 (1996).
25. R. Allmann, *Chimia* **24,** 99–108 (1970).
26. M. Ecker and H. Pöllmann, *Mater. Sci. Forums* **166–169**, 565–570 (1994).
27. S. Auer and H. Pollmann, *J. Solid State Chem.* **109,** 187–196 (1994).
28. S. Miyata, *Clays Clay Miner.* **31,** 305–311 (1983).
29. J. Rodriguez-Carvajal, "FULLPROF, a Program for Rietveld Refinement and Pattern Matching Analysis," 1990.
30. P. Thompson, D. E. Cox, and J. B. Hasting, *J. Appl. Cryst.* **20,** 79–83 (1987).
31. F. Leroux, Y. Piffard, G. Ouvrard, J.-L. Mansot, and D. Guyomard, *Chem. Mater.* **11,** 948–2959 (1999).
32. T. Hibino, Y. Yamashita, K. Kosuge, and A. Tsunashima, *Clays Clay Miner.* **4,** 427 (1995).
33. J. P. Rapin, Materials Science Thesis, University of Nancy, France, 2001.
34. A. Bartos, K. P. Lieb, M. Uhrmacher, and D. Wiarda, *Acta Crystallogr. B* **49,** 165–166 (1993).